REPORT

Effect of temperature variations on the travel time of infiltrating water in the Amsterdam Water Supply Dunes (the Netherlands)

Sida Liu[1] · Yangxiao Zhou[1,2] · Pierre Kamps[3] · Frank Smits[3] · Theo Olsthoorn[3]

Abstract

Travel time is one of the important criteria in the design of managed aquifer recharge systems for securing good drinking water quality. Traditionally, groundwater travel time has been modelled without considering the effect of temperature. In this study, a cross-sectional heat transport model was constructed for the Amsterdam dune filtration system (in the Netherlands) to analyse the effect of temperature on groundwater travel times. A groundwater flow model, a chloride transport model, and a heat transport model were iteratively calibrated with measured groundwater levels, chloride concentrations, and temperature series in order to improve model calibration and reduce model uncertainty. The coupled flow and heat transport model with temperature-dependent density and viscosity provided more accurate estimation of travel times. The results show that seasonal temperature fluctuations in the source water in the infiltration pond cause temperature variations in the shallow groundwater. Viscosity is more sensitive to temperature changes and has a larger effect on groundwater travel times. Groundwater travel time in the shallow sand aquifer increases from 60 days when computed with the traditional groundwater flow model to 73 days in the winter season and 95 days in the summer season when computed with the coupled model. Longer travel time is beneficial for water quality improvement. Thus, it is important to consider the effect of temperature variations on groundwater travel times for the design and operation of managed aquifer recharge systems.

Keywords Groundwater flow · Temperature · Heat transport model · Artificial recharge · The Netherlands

Introduction

Dune filtration systems use natural sand dunes for drinking water storage and production (Dillon 2005). Source water infiltrates from the constructed infiltration ponds and the groundwater is extracted using abstraction canals, underground galleries, and wells. Groundwater travel time between the infiltration and extraction locations plays an important role in the improvement of water quality (Moel et al. 2006). A minimum groundwater travel time is required to satisfy both the water demand and water quality. In the Amsterdam dune infiltration system, in

North Holland (Netherlands), a minimum travel time of 60 days is required to effectively remove pathogens (Olsthoorn 2002). Schijven et al. (2003) showed that the efficiency of pathogen removal depends on flow path length and travel times; the longer the flow path and the residence time, the higher the efficacy of pathogen removal. Derx et al. (2013) found that virus concentration in the abstraction wells increased up to 8 times due to a 30% decrease in travel times.

Groundwater travel time, also known as groundwater residence time, is defined as the time duration between the recharge and discharge of the groundwater in the aquifer system (Loaiciga 2004). It can be estimated by a number of methods, of which several tracer techniques have been widely applied (Cartwright et al. 2017). The radioactive isotopes ^3H, ^{14}C and ^{36}Cl have been used most commonly to determine the groundwater age in different ranges (Moeck et al. 2017; Newman et al. 2010), while other anthropogenic contaminants such as chlorofluorocarbons (CFCs), sulfur hexafluoride (SF6), etc., have also been applied to determine the travel time up to 100 years (Bartyzel and Rozanski 2016, Cook and Solomon 1997). Stable isotope ratios ($\delta^{18}O$ or δ^2H) can also be interpreted by standard lumped parameter

✉ Sida Liu
s.liu@un-ihe.org

1   IHE Delft Institute for Water Education, Westvest 7, 2611 AX Delft, The Netherlands

2   Hebei University of Geosciences, Shijiazhuang City, China

3   Waternet/Amsterdam Water Supply, Vogelenzangseweg 21, 2114 BA Vogelenzang, The Netherlands

models to calculate the groundwater travel time (McGuire and McDonnell 2006); however, the cost for isotope data collection and analysis restrains its application to large -scale problems. Cross-correlation analysis of electrical conductivity time series between the river and monitoring wells was used to estimate average travel times (Sheets et al. 2002), whereas a more rigorous method was to determine travel time distributions by nonparametric deconvolution of electrical conductivity time series (Cirpka et al. 2007). Use of temperature time series to infer groundwater travel times has several advantages (Anderson 2005; Markle and Schincariol 2007; Molina-Giraldo et al. 2011).

Numerical groundwater models have been applied to compute groundwater travel times over several decades (Anderson et al. 2015), as groundwater flow models have the advantage to compute spatial and temporal travel time distributions and can be used as a tool to design the recharge and recovery systems. The widely used computer models were MODFLOW (Harbaugh 2005) in combination with MODPATH (Pollock 1994); however, MODFLOW assumes constant water density and viscosity. It is well known that both density and viscosity are temperature dependent, and there are observed spatial and temporal variations of temperature in groundwater systems. The SEAWAT model (Langevin et al. 2008) can account for temperature-dependent density and viscosity variations in coupled flow and heat transport simulations. Ma and Zheng (2010) investigated the effects of density and viscosity variations on simulating temperature distributions. The effect of temperature variations on groundwater infiltration rate has been studied (Lin et al. 2003; Loizeau et al. 2017; Ronan et al. 1998); however, only a few studies have considered the effect of temperature on estimating groundwater velocities and travel times (Bakker et al. 2015; des Tombe et al. 2018).

In this study, the effect of temperature on travel time computation was investigated, whereby a cross-sectional model was constructed with MODFLOW, MT3DMS and SEAWAT models to simulate the groundwater flow and heat transport from an infiltration pond to an abstraction canal in the Amsterdam Water Supply Dunes. Daily measurements of groundwater level, chloride concentrations, and temperature data were collected to calibrate the groundwater flow, solute and heat transport models. Afterwards, the effects of temperature variations on groundwater level and travel time were investigated with consideration of temperature-dependent density and viscosity in the coupled flow and heat transport model.

Materials and method

Site description

The Amsterdam Water Supply Dunes (AWD) are located 20 km southwest of the city of Haarlem and 1 km south of the town of Zandvoort (Fig. 1). This dunes area (3,600 ha) is

part of the Dutch Western coastal dunes. The Amsterdam Water Supply has been operated in the Amsterdam Dune Area since 1853; however, the abstraction of dune groundwater led to a lowered water table which caused salinization problems (Moel et al. 2006). In 1957, an artificial groundwater recharge system was implemented and helped to mitigate the problem. Treated surface water from River Rhine was infiltrated into the dunes by infiltration ponds.

The surface water is abstracted from the Lekkanaal, a branch of the River Rhine. After pre-treatment with coagulation, sedimentation and rapid sand filtration, it is transported through two pipes, each 50 km long, to the infiltration area in the dunes, where the water is recharged from infiltration ponds and recovered by abstraction canals and drains. Underground drains were constructed between the infiltration ponds to increase water abstraction; these abstraction canals are 40 km long and surround the infiltration area. Functions of the infiltration process include: filtering the bacteria and viruses, filtering the organic and radioactive contaminants, exchanging of heat to maintain a constant groundwater temperature during the whole year, and smoothing of the water quality.

In this study, a cross-section between the infiltration pond No. 6 and the abstraction canal was chosen to investigate the effect of temperature variations on groundwater travel times (Fig. 1). The distance between the infiltration pond and the abstraction canal is 120 m, and along this section are six groundwater monitoring wells (10 J536, P065, P064, P063, P062, 10 J537) and two surface water monitoring points (PK05, PG06). The average water-level elevation is 5.91 m above sea level (asl) at the infiltration pond and 0.75 m at the abstraction canal. The average measured infiltration rate at the infiltration pond No. 6 is about 0.34 m/day. Groundwater levels at monitoring wells are measured manually once per month. Automatic data loggers are installed in the wells 10 J536 (in the fourth screen from the top), P062, PG06 and PK05 for long-term groundwater level and temperature monitoring with hourly frequency (Fig. 2).

Electrical conductivity data of the infiltrated water and abstracted groundwater (represented by groundwater at 10 J536) are collected and converted into the chloride concentrations (Fig. 3) by a regression equation developed specifically for the AWD water (Kamps 2008). Water temperatures are also monitored by temperature loggers at PG06, P062 and 10 J536 (Fig. 4). Since August 2015, extra data loggers measuring groundwater temperature have been installed in every monitoring wells to acquire more temperature data to construct accurate heat transport modelling.

Also analysed was the cross-correlation of the infiltrated water and the abstracted groundwater. Cross correlation could evaluate how two time-series are correlated to each other by shifting one of the time-series with a time lag; thus, by plotting the cross correlation in Eq. (1) with the
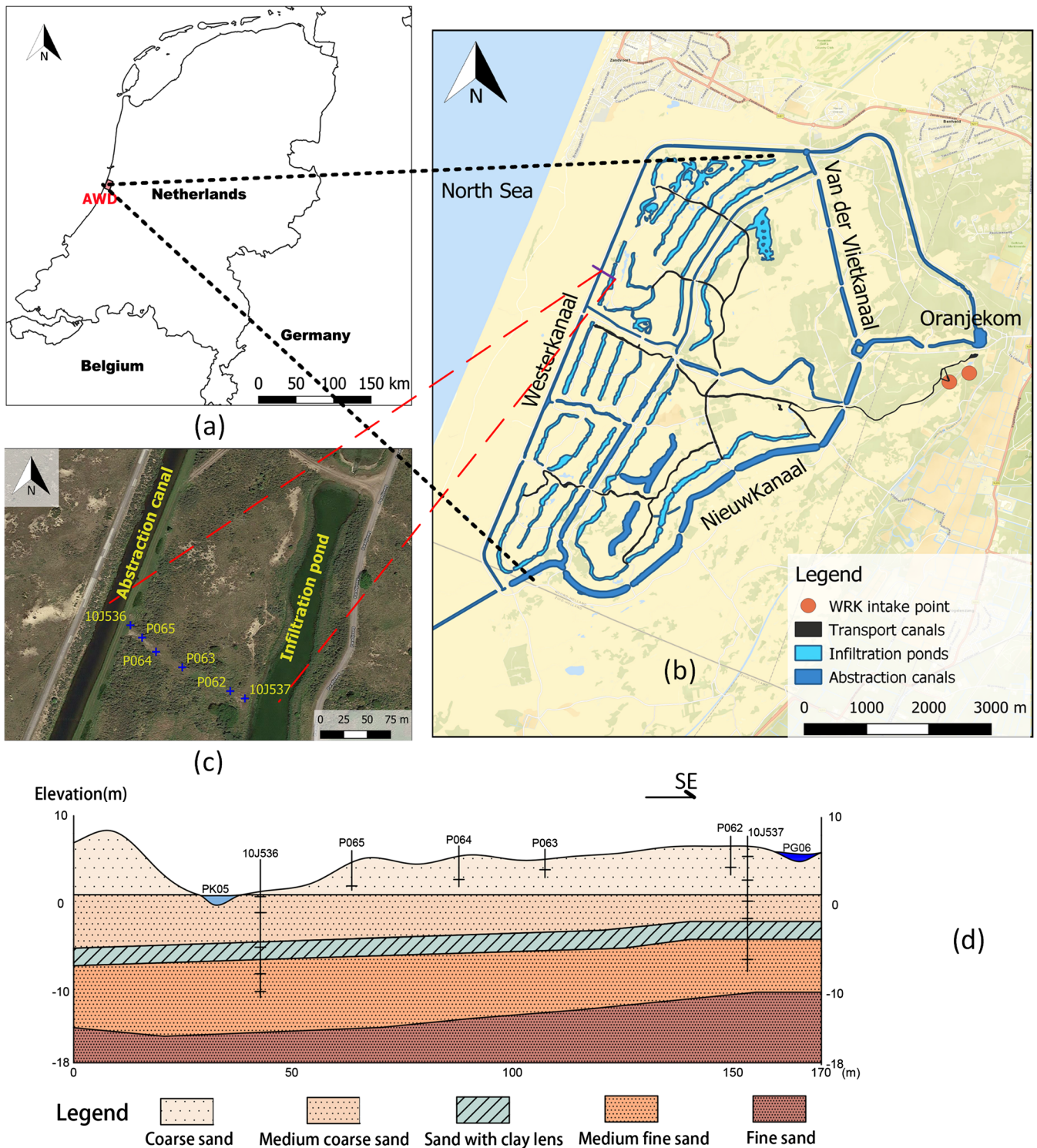
Fig. 1 Location of the study area. **a** Shows the location of the AWD in the Netherlands; **b** shows the map of the study area; **c** shows the location of the selected cross-section and monitoring wells; and **d** is a cross-section map depicting the depth of all monitoring wells—10 J536 and 10 J537 are two multi-level monitoring wells. Other wells only reach the shallow sand aquifer. PG06 monitors water level, temperature and electrical conductivity of the infiltration pond and PK05 monitors water level in the abstraction canal

chloride concentration and temperature data at the infiltration pond and the observation well 10 J536, the conservative solute transport time and the retarded heat transport time can be estimated:
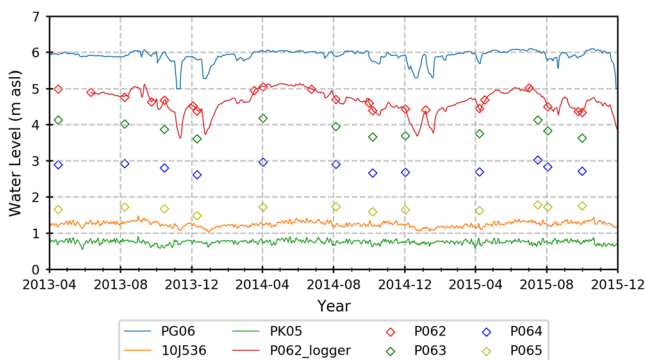
Fig. 2 Surface and groundwater level measurements at all monitoring wells. Points indicate the hand measurements and solid lines are hourly measurements from automatic data loggers

$$r(\tau) = \frac{\sum_i \left[\left(x(i) - \bar{x} \right) \times \left(y(i-\tau) - \bar{y} \right) \right]}{\sqrt{\sum_i \left(x(i) - \bar{x} \right)^2} \times \sqrt{\sum_i \left(y(i) - \bar{y} \right)^2}} \qquad (1)$$

where τ is the time lag. $x(i)$ and $y(i)$ represent the value of the ith element of the time series x and y. $\bar{x}$ and $\bar{y}$ are the mean average of the time series data. The result shows the conservative solute transport time from the infiltration pond to the well 10 J536 is 58 days estimated with Cl time series (Fig. 3). Heat transport time through the aquifer is about 108 days estimated from temperature time series (Fig. 4). These transport times were used to check Cl and heat transport models.

Numerical modelling

MODFLOW 2005 (Harbaugh 2005), MT3DMS (Zheng and Wang 1999) and SEAWAT (Langevin et al. 2008) are widely used for groundwater flow, solute transport, density dependent flow and heat transport modelling. The analogous forms of the solute and heat transport equations were formulated to show how MT3DMS can be also used to simulate heat transport. For a single solute species, the solute transport equation solved by MT3DMS (Langevin et al. 2008) is as follows:

$$\left[1 + \frac{\rho_b K_d}{\theta} \right] \frac{\partial(\theta C)}{\partial t} = \nabla \cdot \left[\theta \left(D_m + \boldsymbol{\alpha} \frac{\boldsymbol{q}}{\theta} \right) \cdot \nabla C \right] - \nabla \cdot (\mathbf{q} C) - q'_s C_s \qquad (2)$$
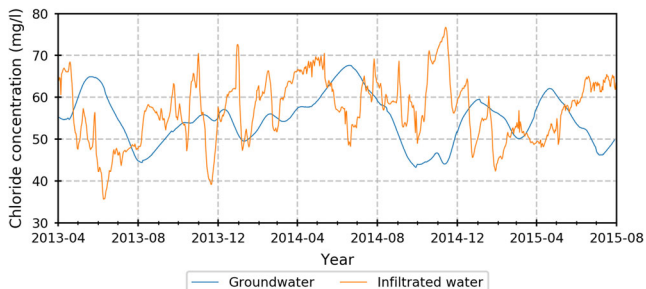

Fig. 3 Chloride concentrations of the source water in the infiltration pond PG06 and groundwater at the well 10 J536 next to the abstraction canal from April 2013 to July 2015
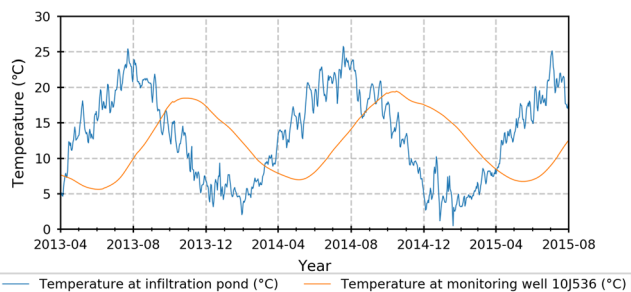
Fig. 4 Water temperature measurements in the infiltration pond PG06 and the observation well 10 J536 from April 2013 to July 2015

where the following terms are as defined:

ρ_b Bulk density (mass of the solids divided by the total volume) [ML^{-3}]
K_d Distribution coefficient of solute [L^3 M^{-1}]
θ Porosity [−]
C Concentration of solute [ML^{-3}]
∇ Vector differential operator
D_m Molecular diffusion coefficient [L^2 T^{-1}]
$\boldsymbol{\alpha}$ Dispersivity tensor [L]
$\mathbf{q}$ Specific discharge vector [LT^{-1}]
C_s Source concentration of solute [ML^{-3}]

For conservative solutes like Cl, there is no sorption so that the distribution coefficient is zero. The molecular diffusion is much smaller than dispersion and can be neglected. The dispersion tensor depends on longitudinal and transversal dispersivities.

The analogous equation for heat transport is defined as:

$$\left[1 + \frac{1-\theta}{\theta} \frac{\rho_s c_{Psolid}}{\rho\, c_{Pfluid}} \right] \frac{\partial(\theta T)}{\partial t} = \nabla \cdot \left[\theta \left(\frac{K_{Tbulk}}{\theta \rho c_{Pfluid}} + \boldsymbol{\alpha} \frac{\boldsymbol{q}}{\theta} \right) \cdot \nabla T \right] - \nabla \cdot (\mathbf{q} T) - q'_s T_s \qquad (3)$$

where the following definitions apply:

T Temperature [°C]
ρ_s Density of the solid [ML^{-3}]
c_{Psolid} Specific heat capacity of the solid [L^2 T^{-2} °C^{-1}]
c_{Pfluid} Specific heat capacity of the fluid [L^2 T^{-2} °C^{-1}]
∇ Vector differential operator
K_{Tbulk} Bulk thermal conductivity of the aquifer material [ML^3 T^{-2} °C^{-1}]
T_s Source temperature [°C]

When MT3DMS is used to simulate heat transport, the equivalent transport parameters are defined. For simulating heat exchange between solid and groundwater, a thermal distribution factor is defined as:

$$K_{d\_temp} = \frac{c_{Psolid}}{\rho c_{Pfluid}} \qquad (4)$$

The equivalent heat retardation factor can be computed as:

$$R_\text{d} = 1 + \frac{(1-\theta)\rho_\text{s} K_{\text{d\_temp}}}{\theta} \quad (5)$$

The heat conduction term in Eq. (3) is equivalent to the molecular diffusion in Eq. (2), so a thermal diffusivity is defined as:

$$D_{\text{m\_temp}} = \frac{K_\text{Tbulk}}{\theta \rho c_\text{Pfluid}} \quad (6)$$

The bulk thermal conductivity is computed as:

$$K_\text{Tbulk} = \theta K_\text{Tfluid} + (1-\theta) K_\text{Tsolid} \quad (7)$$

The heat dispersion is the same as solute dispersion determined by the longitudinal and transversal dispersivities.

The specific discharge vector is computed by MODFLOW with Darcy's equation and depends on the hydraulic conductivity defined as:

$$K = \frac{k\rho g}{\mu} \quad (8)$$

where the following parameters correspond to:

K Hydraulic conductivity $[\text{LT}^{-1}]$
κ Intrinsic permeability $[\text{L}^2]$
μ Dynamic viscosity $[\text{ML}^{-1}\,\text{T}^{-1}]$
g   Gravitational acceleration $[\text{LT}^{-2}]$

For heat transport modelling, the hydraulic conductivity varies according to changes of density and viscosity in relation to changes in temperature. The approximate equations for relations between the density and viscosity and temperature are estimated as (des Tombe et al. 2018):

$$\rho_\text{w}(T) = 999.1 - 0.1125 \cdot (T-12) \quad (9)$$

$$\mu(T) = 10^{-3} \cdot \left[1 + 1.55 \cdot 10^{-2} \cdot (T-20)\right]^{-1.572} \quad (10)$$

The groundwater temperature at the study site varies between roughly 5 and 20 °C. Equation (9) gives a change in the water density of only 0.16%, while Eq. (10) computes the viscosity change with 34%. This results in a 51% higher hydraulic conductivity value for water of 20 °C compared with water of 5 °C (Eq. 8); therefore, the density-driven flow can be neglected, while the effect of viscosity must be included. Although MT3DMS does not consider the viscosity changes, SEAWAT has a viscosity package (VSC) to consider the effect of viscosity changes. Since temperature has these effects on both flow and heat transport, the coupled flow and heat transport should be modelled with SEAWAT.

The modelled domain is a cross-section of 450 and 32 m depth (Fig. 5). The cross-section consists of mainly two sub-areas, divided by the abstraction canal where the lowest water level is found. The west sub-area is the natural coastal sand dunes where the main recharge source is precipitation (about
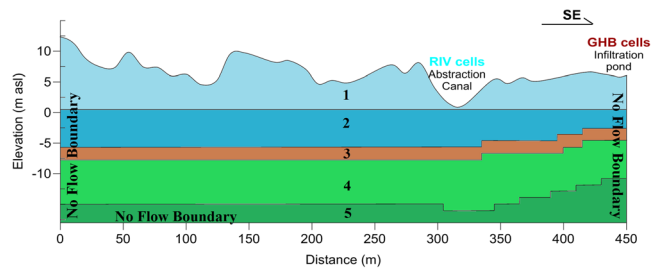

Fig. 5 Five parameter zones and boundary conditions of the cross-section model

1 mm/day). The west boundary is a groundwater divide which divides groundwater discharge to the North Sea in the west side and groundwater discharge to the abstraction canal in the east side. The water table in this area is very stable and has a flat hydraulic gradient. The east sub-area is the infiltration area where the main source of water is the infiltrated water from the infiltration pond. The measured infiltration rate is about 0.34 m/day, which is much higher than natural groundwater recharge from precipitation. The east boundary is also a groundwater divide formed by the infiltration pond. The boundary is chosen at the centre line of the pond which divides infiltrated water flowing to the abstraction canal and the underground drain.

According to the borehole data of the monitoring wells 10 J536 and 10 J537, the cross-section can be divided into five parameter zones vertically (Fig. 5). Zones 1 and 2 represent the shallow sandy unconfined aquifer, zone 3 represents a thin silty clay layer lying in the middle of the aquifer which influences the flow pattern significantly, while zones 4 and 5 represent the lower sandy confined aquifer. The bottom of the aquifer consists of a thick clay layer and was defined as a no-flow boundary. All hydraulic parameters and thermal parameters were assigned to each parameter zone. Table 1 lists the calibrated values.

The numerical model consists of 90 columns with a uniform size of 5 m and 32 model layers with a uniform layer thickness of 1.0 m. The model grid size is sufficiently small to accommodate aquifer geometry, heterogeneity, spatial variations of groundwater levels, Cl concentrations and temperatures, and boundary conditions. The general head boundary (GHB) package was used to simulate the infiltration pond. The measured water levels and hydraulic conductance of the pond were specified to compute infiltration rate. River (RIV) package was used to simulate the abstraction canal. The measured water levels and hydraulic conductance of the canal were specified to compute groundwater discharge to the canal. Recharge (RCH) package was used to simulate the natural groundwater recharge from precipitation. Both the west and east boundaries were simulated as no-flow boundaries since groundwater divides exist, and the bottom boundary was simulated also as a no-flow boundary.

Table 1 Parameterization of the groundwater flow and heat transport model

Parameter	Unit	Parameter zone				
		1	2	3	4	5
Horizontal hydraulic conductivity	m/day	11.40	8.55	0.48	5.70	4.75
Vertical hydraulic conductivity	m/day	3.42	2.00	0.14	1.71	1.43
Effective porosity	–	0.19	0.15	0.10	0.24	0.25
Longitudinal dispersivity	m	2.73	1.28	0.14	1.09	0.91
Transversal dispersivity	m	0.27	0.13	0.01	0.11	0.09
Bulk density	kg/m^3	1,850	1,850	1,100	1,850	1,850
Specific heat capacity of solids	J/(kg °C)	226	226	1,214	1,101	1,101
Specific heat capacity of water	J/(kg °C)	4,186	4,186	4,186	4,186	4,186
Thermal distribution factor	m^3/kg	5.41×10^{-5}	5.41×10^{-5}	2.9×10^{-3}	2.63×10^{-4}	2.63×10^{-4}
Thermal conductivity of solids	W/(m °C)	1.091	0.821	0.323	0.936	0.988
Thermal conductivity of water	W/(m °C)	0.58	0.58	0.58	0.58	0.58
Bulk thermal diffusivity	m^2/day	0.096	0.096	0.06	0.0612	0.0612
Hydraulic conductance	General head boundary: 15 m^2/day					
	Riverbed: 250 m^2/day					

An iterative model construction and calibration procedure was used in this study. First, a steady-state groundwater flow model was constructed with MODFLOW. The flow model was preliminarily calibrated with groundwater level measurements and measured infiltration rate from the infiltration pond. The main parameters calibrated were hydraulic conductivities in five parameter zones; secondly, the Cl transport model was constructed and calibrated using MT3DMS with measured Cl concentration time series in observation wells. The peak Cl concentration travels with the average groundwater velocity which was computed with MODFLOW model. Transport parameters such as longitudinal and transversal dispersivities are not associated with the Cl concentration flow path. When the computed peak Cl concentration did not match the measured concentration, the groundwater flow model was recalibrated. Thirdly, the heat transport model was constructed and calibrated using SEAWAT with temperature measurements. Parameters for heat conduction (thermal conductivity or thermal diffusivity) and heat exchange (thermal distribution factor) were mainly calibrated. When computed peak temperature did not match the measured peak in observation wells, the flow and Cl transport model were further recalibrated.

Results

Flow model calibration

The groundwater flow model is of great importance since it computes cell-by-cell specific discharges which are used for convective transport modelling of Cl and heat transport. Since the infiltration system was under stable operation in the period

from April 1, 2013 to December 31, 2015 (see Fig. 2), a steady-state flow model was constructed by taking average values of the recharge and water levels of the pond and the canal in this period. The steady-state flow model was preliminarily calibrated from two perspectives: (1) comparing the computed groundwater levels with the measured groundwater levels from the observation wells; (2) matching the computed inflow from the infiltration pond to the measured average infiltration rate. The calibrated parameters were hydraulic conductivities and hydraulic conductance of the pond and the
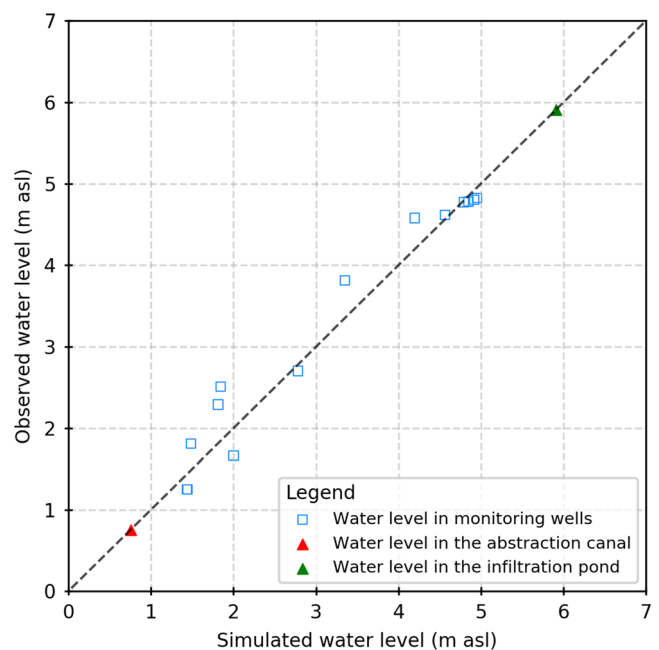
Fig. 6 Scatter plot of the computed and observed groundwater levels from the observation wells

canal. The parameter optimization code PEST (Doherty 2016) was used to automatically calibrate the parameter values.

The average groundwater levels at all monitoring wells were used for the model calibration. Figure 6 is the scatter diagram of the computed versus the observed groundwater levels. The average difference between computed and observed groundwater level is 0.016 m with a standard deviation of 0.06 m. The computed inflow from the infiltration pond is 0.36 m/day, which is close to the measured infiltration rate (0.34 m/day). Generally, the model accuracy is acceptable.

The spatial distribution of groundwater levels simulated with the steady-state flow model is shown in Fig. 7. The water table at the natural coastal sand dune is relatively flat and around 1.5 m. At the artificial recharge area, the groundwater level varies from 5.9 m at the infiltration pond to 0.5 m beneath the abstraction canal.

Groundwater travel time was computed with MODPATH (Pollock 1994). In total, 40 particles were set at the abstraction canal and tracked backward until arriving at the infiltration pond (Fig. 7). Particles flowing through the shallow sand aquifer have shorter travel times. The minimum travel time at the shallow sand layer is only 59 days. The particles travel vertically through the middle silty clay layer causing refraction of flow lines. Particles travel through the lower sandy aquifer resulting in longer travel times. The maximum travel time could reach 262 days, whereas the average travel time of the 40 particles is about 127 days.

Solute transport model calibration

The long-term continuous measurements of Cl concentrations (Fig. 3) provided opportunity to construct a Cl transport model to constrain flow model calibration and to calibrate transport parameters. The simulation period is from April 1, 2013 to December 26, 2015 for 1,000 days with a daily stress period. The transport step size is determined automatically by MT3DMS according to the convergence criteria. The infiltration pond is the source of Cl and daily Cl measurements was specified in the GHB package to simulate the source input. The new parameters for the Cl transport model, which were also optimized with PEST code, are effective porosity and longitudinal and transversal dispersivities (Table 1).
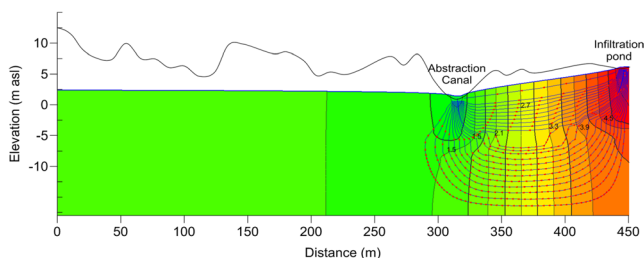

Fig. 7 Simulated groundwater level and flow lines of the steady-state flow model

Firstly, a pulse of Cl concentration was specified at the infiltration pond (100 mg/L), and the breakthrough curve at the observation well (10 J536) was simulated. Figure 8a shows that the peak Cl concentration arrives at well 10 J536 in 61 days, indicating the average convective transport time. This average convective travel time (61 days) compares well to the travel time estimated with the cross-correlation of Cl time series (58 days) and the travel time computed with MODPATH (59 days).

Secondly, the actual Cl transport model was constructed with daily Cl concentrations at the infiltration pond (Fig. 3) specified as the external source. The initial Cl concentrations were not available and were determined iteratively. An average Cl concentration of 55 mg/L was used as initial concentration; then, the transport model was run and the computed Cl concentrations in April 1, 2014 were used as the new initial condition, since Cl measurements in April 1, 2013 are very close to Cl measurements in April 1, 2014. After a few iterations, the computed initial conditions became stable and the influence of the initial conditions disappeared. The goodness of fit was checked for all observation wells with Cl measurements. Figure 8b plots the measured and computed Cl concentrations at observation well 10 J536. Though there are some gaps in peak values, the simulated Cl concentrations mimic the variations of the measured values with a very high correlation coefficient of 0.95.

Heat transport model calibration and result

The heat transport model was constructed based on the Cl transport model. The simulation period is the same from April 1, 2013 to December 26, 2015 for 1,000 daily stress periods. The heat transport model includes the convective transport, dispersive transport, heat conduction, and heat exchange, while for the heat transport model calibration, the density and viscosity were assumed constant. The effect of
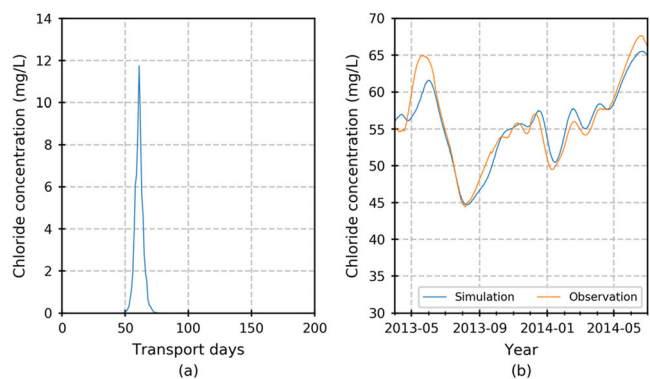

Fig. 8 Calibration of the Cl solute transport model. **a** Shows the result of the impulse response model; **b** shows the comparison of the simulated and observed chloride concentrations of the continuous solute transport model at the observation well 10 J536
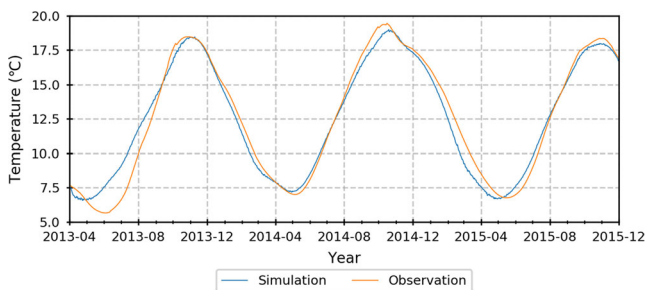
Fig. 9 Computed and measured groundwater temperature series at the observation well 10 J536

temperature variations on heat transport and travel times is discussed in the next section.

The heat convective transport resembles the solute transport while there are different opinions regarding the heat and solute dispersive transport (Vandenbohede et al. 2009). In this study, the same dispersive parameters from the Cl transport model were used for heat dispersive transport simulation. For heat conduction, the equivalent thermal diffusivity (Eq. 6) was specified and simulated with MT3DMS Species-Dependent Diffusion package. The heat exchange was simulated as equivalent sorption reaction defined by an equivalent thermal distribution factor (Eq. 5) and was simulated with MT3DMS Chemical

Reaction package. These two lumped thermal parameters and related basic thermal parameters are listed in Table 1.

The infiltration pond is an external heat source. The daily water temperature measurements from the pond were specified in the GHB package as the source temperature (Fig. 4), while the average daily air temperature was specified in the recharge package to simulate ground temperature influence. The same iterative procedure was used to compute initial temperature conditions. An average groundwater temperature of 12 °C was assigned as the initial condition and the heat transport model was run to compute temperature distribution in April 1, 2014, which was subsequently used as the new initial condition. This procedure was repeated a few times to create a stable initial condition.

The comparison of computed and measured temperature series at the observation well 10 J536 is plotted in Fig. 9. The result shows the heat transport model simulates groundwater temperature variations very well at the observation well 10 J536.

The heat front moves slower than the average groundwater flow velocity due to the effect of "retardation" caused by heat exchange between the groundwater and soil medium. The simulated average groundwater temperature under the abstraction canal is 12.56 °C. The highest temperature occurs between October and

Fig. 10 Computed groundwater levels **a** beneath the infiltration pond, and **b** next to the abstraction canal, with the steady-state flow model (blue line), the coupled model with only density effect (brown line) and the viscosity and density effect (green line)
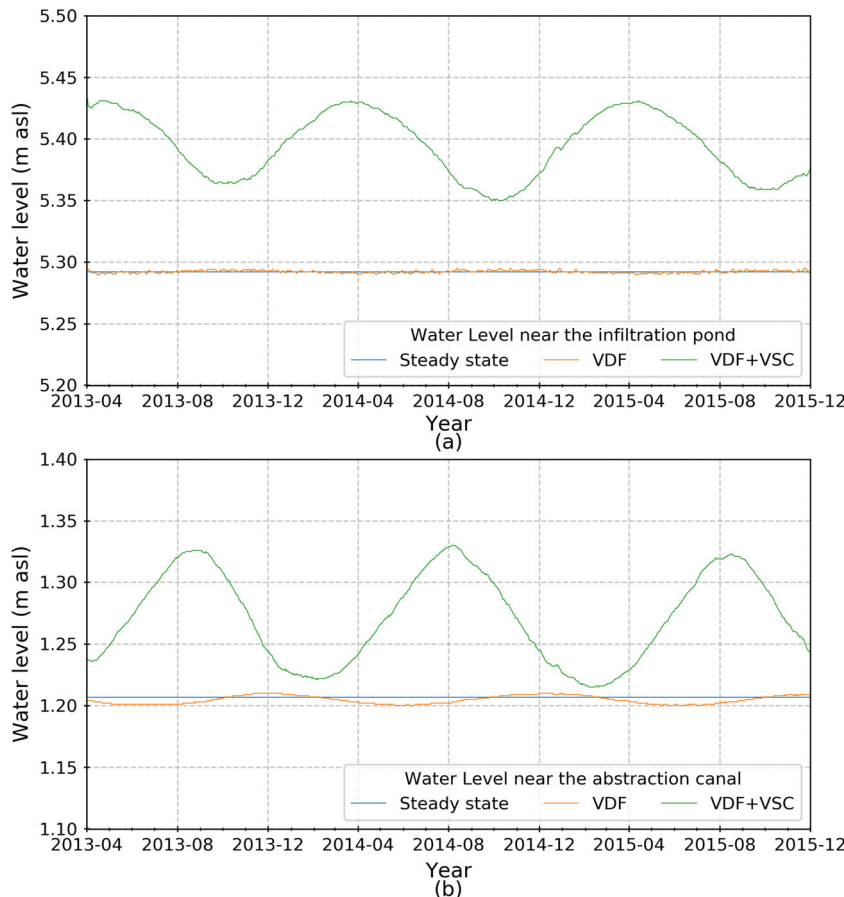
November every year around 18 °C and the lowest temperature is in April and May around 7 °C. During the summer time, warmer water with a temperature of about 25 °C infiltrates into the aquifer; due to the retardation effect, higher groundwater temperature occurs at the abstraction canal during the winter time.

Effect of temperature variations

Groundwater density and viscosity change in response to temperature variations (Eqs. 9 and 10). Both density and viscosity decrease with the increase of temperature; however, hydraulic conductivity is proportional to density changes and inversely proportional to viscosity changes (Eq. 8). The effect of temperature variations on groundwater flow and heat transport was investigated with the coupled flow and heat transport model using SEAWAT. The Variable-Density Flow (VDF) package and the Viscosity (VSC) package were used to incorporate density and viscosity changes in response to temperature changes. In the coupled flow and heat transport model with SEAWAT, flow and heat transport equations are solved iteratively at every transport step while updating hydraulic conductivity values corresponding to temperature-dependent density and viscosity. Therefore, although flow boundary conditions are constant, SEAWAT computes transient groundwater levels and specific discharges (velocities) induced by temperature changes. The simulation period is the same from April 1, 2013 to December 26, 2015 for 1000 daily stress periods.

Effect of temperature variations on groundwater levels

The computed groundwater levels with the steady-state flow model (MODFLOW) and the coupled flow and heat transport model (SEAWAT) were compared to evaluate the effects of the density and viscosity changes caused by temperature variations. Figure 10 plots computed groundwater levels beneath the infiltration pond (Fig. 10a) and next to the abstraction canal (Fig. 10b). In general, density has a minor effect on computed groundwater levels. The computed groundwater levels with temperature-dependent viscosity are higher than groundwater levels computed with the steady-state flow model. The reason for this is that the temperature in the model site is always lower than the reference temperature (25 °C) resulting in smaller hydraulic conductivity values in the coupled flow and heat transport model; furthermore, seasonal variations of temperature in the infiltration pond cause the seasonal change of groundwater levels with some phase shift.
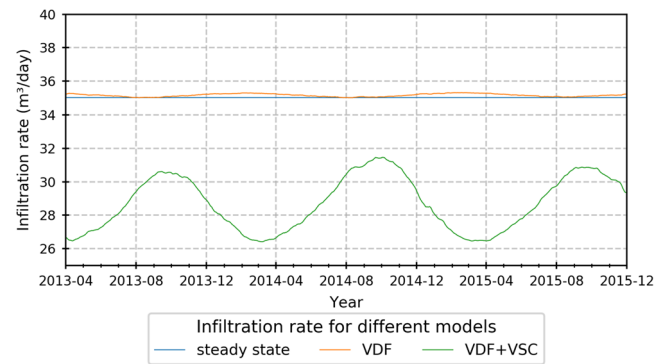

Fig. 11 Computed infiltration rates with the steady-state flow model (blue line), the coupled model with only density effect (brown line) and the viscosity and density effect (green line)

Effect of temperature variations on infiltration rate

The effect of temperature variations on groundwater levels has consequences on computing infiltration rate from the infiltration pond (Fig. 11). The computed infiltration rate from the coupled model is lower than that computed from the steady-state flow model. The viscosity has a larger effect than the density; furthermore, the computed infiltration rate is higher in summer season under higher temperature, and lower in the winter season under lower temperature.

Effect of temperature variations on travel times

The effects of temperature variations on groundwater travel times were evaluated and compared with consideration of only the density effect (VDF) and viscosity effect (VSC). The coupled flow and heat transport model computed daily groundwater velocities from April 1, 2013 to December 26, 2015, induced by temperature-dependent density and viscosity changes. For particle tracking with MODPATH, the transient flow velocity was used to move particles at every transport step. The starting date of particle tracking was varied daily from June 1, 2014 to May 31, 2015. For each starting date, 40 particles placed at the abstraction canal were tracked
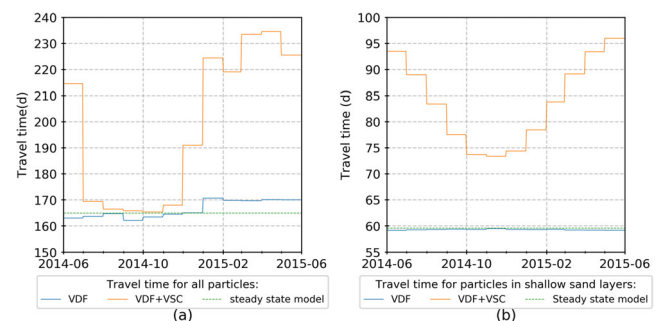

Fig. 12 Comparison of the groundwater travel times with and without considering the effect of temperature: **a** shows the comparison when all particles are considered., **b** shows the comparison for pathlines in the shallow sand aquifer

backward until arriving at the infiltration pond, whereby each particle had its own pathline and travel time. The average travel time of 40 particles was computed as the representation of the travel time for the starting date of the particle tracking, which was how Fig. 12 was prepared. Figure 12a shows the average groundwater travel times for all 40 particles, while Fig. 12b presents the average groundwater travel times only for particles in the shallow sandy aquifer.

From both figures, the density effect on travel times is minor; however, viscosity has a large effect on the travel time. Since groundwater temperature varies between 5 and 20 °C in the aquifer, the difference in density change is less than 1.0%, while the change in viscosity is more than 34.0%. Furthermore, since groundwater temperature is lower than the reference temperature of 25 °C, the hydraulic conductive is smaller than the value at the reference temperature, resulting in longer travel times. Groundwater in the shallow sand aquifer above the middle silty clay layer is critical to the water quality since it has the shortest travel time. The average travel time is about 60 days computed from the steady-state MODFLOW model and the heat transport model only with density effect (Fig. 12b), merely satisfying the travel time requirement for artificial recharge; however, average travel time increases largely when the viscosity effect is considered. In the winter season, the average travel time is lower, about 73 days, because warmer recharged water travelled into the shallow aquifer, whereas in the summer season, the average travel time is higher, up to 95 days, because the colder recharged water occupies the shallow aquifer.

Conclusions

Travel time is a very important criterion in the design and operation of the managed aquifer recharge system. In the design of the recharge and abstraction schemes, a numerical groundwater flow model is usually used to compute travel times from the recharge locations to the extraction points; however, the effect of temperature on travel times was not considered.

This study demonstrates that temperature has a large effect on travel time via viscosity changes. Only considering density dependence on the temperature variations is not sufficient to accurately compute travel times. Viscosity dependence on temperature changes must be considered since viscosity is more sensitive to temperature changes. In the colder climate where groundwater temperature is usually lower than the reference temperature of 25 °C, groundwater travel time could be underestimated with the groundwater flow model without considering viscosity effect. In the Amsterdam dune water area, groundwater travel times in the shallow sand aquifer increased from 60 to 73 days in the winter season and to 95 days in the summer season. These results provide higher confidence in the recharge system since longer travel time results in most likely better water quality.

However, in a tropical climate where groundwater temperature is higher than the reference temperature, groundwater travel time could be overestimated with the groundwater flow model without considering the viscosity effect. In this case, there is a risk of insufficient water quality improvement since actual travel time is less than the desired travel time requirement. It is more critical in tropical climate areas to use the coupled flow and heat transport model with viscosity effect to compute groundwater travel times.

References

Anderson MP (2005) Heat as a ground water tracer. Ground Water 43: 951–968. https://doi.org/10.1111/j.1745-6584.2005.00052.x

Anderson MP, Woessner WW, Hunt RJ (2015) Applied groundwater modeling: simulation of flow and advective transport. Academic, San Diego

Bakker M, Caljé R, Schaars F, van der Made K-J, de Haas S (2015) An active heat tracer experiment to determine groundwater velocities using fiber optic cables installed with direct push equipment. Water Resour Res 51:2760–2772

Bartyzel R (2016) Dating of young groundwater using four anthropogenic trace gases (SF6, SF5CF3, CFC-12 and Halon-1301): methodology and first results. Isot Environ Health Stud 52:393–404. https://doi.org/10.1080/10256016.2015.1135137

Cartwright I, Cendón D, Currell M, Meredith K (2017) A review of radioactive isotopes and other residence time tracers in understanding groundwater recharge: possibilities, challenges, and limitations. J Hydrol 555:797–811

Cirpka OA, Fienen MN, Hofer M, Hoehn E, Tessarini A, Kipfer R, Kitanidis PK (2007) Analyzing bank filtration by deconvoluting time series of electric conductivity. Groundwater 45:318–328

Cook PG, Solomon DK (1997) Recent advances in dating young groundwater: chlorofluorocarbons, and 85Kr. J Hydrol 191:245–265. https://doi.org/10.1016/S0022-1694(96)03051-X

Derx J, Blaschke A, Farnleitner A, Pang L, Blöschl G, Schijven J (2013) Effects of fluctuations in river water level on virus removal by bank filtration and aquifer passage: a scenario analysis. J Contam Hydrol 147:34–44

des Tombe BF, Bakker M, Schaars F, van der Made KJ (2018) Estimating travel time in Bank filtration systems from a numerical model based on DTS measurements. Groundwater 56:288–299

Dillon P (2005) Future management of aquifer recharge. Hydrogeol J 13: 313–316. https://doi.org/10.1007/s10040-004-0413-6

Doherty J (2016) PEST Model-independent parameter estimation user manual Part I: PEST, SENSAN and global optimisers. Watermark numerical computing 6

Harbaugh AW (2005) MODFLOW-2005, the US Geological Survey modular ground-water model: the ground-water flow process. US Geological Survey, Reston, VA

Kamps PTWJ (2008) Methoden van kartering van zoet, brak en zout grondwater in de Amsterdamse Waterleidingduinen [Methods for mapping fresh, brackish and saline groundwater inthe Amsterdam Water Supply Dunes]. Internal report, Waternet, Amsterdam, 33 pp

Langevin CD, Thorne Jr DT, Dausman AM, Sukop MC, Guo W (2008) SEAWAT version 4: a computer program for simulation of multi-species solute and heat transport. US Geological Survey, Reston, VA

Lin CY, Greenwald D, Banin A (2003) Temperature dependence of infiltration rate during large scale water recharge into soils. Soil Sci Soc Am J 67:487–493

Loaiciga H (2004) Residence time, groundwater age, and solute output in steady-state groundwater systems. Adv Water Resour 27(7):681–688

Loizeau S, Rossier Y, Gaudet JP, Refloch A, Besnard K, Angulo-Jaramillo R, Lassabatere L (2017) Water infiltration in an aquifer recharge basin affected by temperature and air entrapment. J Hydrol Hydromech 65:222–233. https://doi.org/10.1515/johh-2017-0010

Ma R, Zheng C (2010) Effects of density and viscosity in modeling heat as a groundwater tracer. Groundwater 48:380–389

Markle JM, Schincariol RA (2007) Thermal plume transport from sand and gravel pits–potential thermal impacts on cool water streams. J Hydrol 338:174–195

McGuire KJ, McDonnell JJ (2006) A review and evaluation of catchment transit time modeling. J Hydrol 330:543–563. https://doi.org/10.1016/j.jhydrol.2006.04.020

Moeck C, Radny D, Popp A, Brennwald M, Stoll S, Auckenthaler A, Berg M, Schirmer M (2017) Characterization of a managed aquifer recharge system using multiple tracers. Sci Total Environ 609:701–714. https://doi.org/10.1016/j.scitotenv.2017.07.211

Moel PJ, Verberk JQ, Van Dijk J (2006) Drinking water: principles and practices. World Scientific, Singapore

Molina-Giraldo N, Bayer P, Blum P, Cirpka OA (2011) Propagation of seasonal temperature signals into an aquifer upon bank infiltration. Groundwater 49:491–502

Newman BD, Osenbrück K, Aeschbach-Hertig W (2010) Dating of 'young' groundwaters using environmental tracers: advantages, applications, and research needs. Isot Environ Health Stud 46:259–278

Olsthoorn T (2002) Fifty years artificial recharge in the Amsterdam dune area. In: Management of aquifer recharge for sustainability. Netherlands National Committee for the IAHin cooperation with Netherlands Hydrological Society, Delft, The Netherlands

Pollock DW (1994) User's guide for MODPATH/MODPATH-PLOT, version 3: a particle tracking post-processing package for MODFLOW: the US Geological Survey finite-difference groundwater flow model. US Geol Surv Open-File Rep 94-464

Ronan AD, Prudic DE, Thodal CE, Constantz J (1998) Field study and simulation of diurnal temperature effects on infiltration and variably saturated flow beneath an ephemeral stream. Water Resour Res 34:2137–2153. https://doi.org/10.1029/98wr01572

Schijven J, De Bruin H, Hassanizadeh S, de Roda Husman A (2003) Bacteriophages and clostridium spores as indicator organisms for removal of pathogens by passage through saturated dune sand. Water Res 37:2186–2194

Sheets R, Darner R, Whitteberry B (2002) Lag times of bank filtration at a well field, Cincinnati, Ohio, USA. J Hydrol 266:162–174

Vandenbohede A, Louwyck A, Lebbe L (2009) Conservative solute versus heat transport in porous media during push-pull tests. Transp Porous Media 76:265–287

Zheng C, Wang PP (1999) MT3DMS: a modular three-dimensional multispecies transport model for simulation of advection, dispersion, and chemical reactions of contaminants in groundwater systems: documentation and user's guide DTIC document. US Army Corps of Engineers, Washington, DC